APPLIED SCIENCES AND ENGINEERING

Fluorescent-based biodegradable microneedle sensor array for tether-free continuous glucose monitoring with smartphone application

Mingyu Sang[1]†, Myeongki Cho[1]†, Selin Lim[1,2]†, In Sik Min[1]†, Yuna Han[3,4], Chanwoo Lee[1], Jongwoon Shin[1], Kukro Yoon[5], Woon-Hong Yeo[6], Taeyoon Lee[5], Sang Min Won[7], Youngmee Jung[2,8]*, Yun Jung Heo[3,4]*, Ki Jun Yu[1,2]*

Continuous glucose monitoring (CGM) allows patients with diabetes to manage critical disease effectively and autonomously and prevent exacerbation. A painless, wireless, compact, and minimally invasive device that can provide CGM is essential for monitoring the health conditions of freely moving patients with diabetes. Here, we propose a glucose-responsive fluorescence-based highly sensitive biodegradable microneedle CGM system. These ultrathin and ultralight microneedle sensor arrays continuously and precisely monitored glucose concentration in the interstitial fluid with minimally invasive, pain-free, wound-free, and skin inflammation–free outcomes at various locations and thicknesses of the skin. Bioresorbability in the body without a need for device removal after use was a key characteristic of the microneedle glucose sensor. We demonstrated the potential long-term use of the bioresorbable device by applying the tether-free CGM system, thus confirming the successful detection of glucose levels based on changes in fluorescence intensity. In addition, this microneedle glucose sensor with a user-friendly designed home diagnosis system using mobile applications and portable accessories offers an advance in CGM and its applicability to other bioresorbable, wearable, and implantable monitoring device technology.

INTRODUCTION

According to the International Diabetes Federation, the number of patients with diabetes worldwide is 536.6 million, i.e., 10.5% of the total population, and is expected to increase to more than 783.2 million individuals by 2045 (*1*–*3*). In particular, hypoglycemia is a serious condition that can cause behavioral and cognitive impairment, seizures, loss of consciousness, coma, brain damage, or death. In addition to the severity of diabetes itself, this condition can also cause serious medical complications in other organs, such as the kidneys, liver, and heart. Moreover, the incidence of complications is extremely high, and 11.3% of the worldwide mortality rate is attributable to diabetes. Most of these deaths occur under the age of 60, and the mortality rate is expected to increase further if adequate management or treatment is not provided (*4*–*7*). Diabetes requires constant management to avoid unfortunate consequences, such as death. Therefore, precise monitoring of the blood-glucose level in the body, which is an important indicator for managing type 1 and type 2 diabetes, is necessary. By managing blood glucose, patients with diabetes can gain health physiological insights and effectively and actively control this fatal disease. Currently, the lancet diagnostic method is the blood-glucose measurement approach that is used most widely (*8*); however, this is an invasive, blood-collecting procedure in which a needle containing a glucose oxidase enzyme is used to prick the tip of a finger. Despite the high accuracy of the lancet method, it is accompanied by pain, skin damage, wounding, and the possibility of bacterial invasion; moreover, it cannot provide continuous blood-glucose concentration information, which is a critical drawback that precludes the prevention of hypoglycemia or hyperglycemia (*9*).

Continuous glucose monitoring (CGM) is crucial for tracking blood-glucose levels in real-time, providing critical information to effectively prevent diabetic complications arising from hypo- or hyperglycemic episodes (*10*). While invasive lancet measurement is not compatible with CGM, commercial and research efforts have been directed toward developing biosensors for CGM. Commercial efforts have made great progress in glucose monitoring technology, with currently available first- and second-generation CGMs including semi-implantable needle-typed sensors that use glucose oxidase and fully implantable radio frequency (RF) sensors that incorporate boronic acids (*11*). Although CGM with glucose oxidase–immobilized electrodes has reached to zero blood-collection calibration, it still has discomfort from the attached transmitter on skin, infection risk through the open wound, and a short life span of up to 14 days (*12*–*16*). In contrast, boronic acid–based glucose sensor is the newer sensor that does not require any enzyme or reagent to sense glucose,

[1]Functional Bio-integrated Electronics and Energy Management Lab, School of Electrical and Electronic Engineering, Yonsei University, 50 Yonsei-ro, Seodaemun-gu, Seoul 03722, Republic of Korea. [2]Department of Electrical and Electronic Engineering, YU-Korea Institute of Science and Technology (KIST) Institute, Yonsei University, 50 Yonsei-ro, Seodaemun-gu, Seoul 03722, Republic of Korea. [3]Department of Mechanical Engineering, Kyung Hee University, 1732 Deogyeong-daero, Yongin-si, Gyeonggi-do 17104, Republic of Korea. [4]Integrated Education Institute for Frontier Science & Technology (BK21 Four), Kyung Hee University, 1732 Deogyeong-daero, Yongin-si, Gyeonggi-do 17104, Republic of Korea. [5]NanoBio Device Laboratory, School of Electrical and Electronic Engineering, Yonsei University, 50 Yonsei-ro, Seodaemungu, Seoul 03722, Republic of Korea. [6]Bio-Interfaced Translational Nanoengineering Group, George W. Woodruff School of Mechanical Engineering, Georgia Institute of Technology, Atlanta, GA 30332, USA. [7]Flexible Electronic System Research Group, Department of Electrical and Computer Engineering, Sungkyunkwan University, 2066 Seobu-ro, Jangan-gu, Suwon-si, Gyeonggi-do, Republic of Korea. [8]Center for Biomaterials, Biomedical Research Institute, Korea Institute of Science and Technology (KIST), Seoul 02792, Republic of Korea.
*Corresponding author. Email: winnie97@kist.re.kr (Y.J.); yunjheo@khu.ac.kr (Y.J.H.); kijunyu@yonsei.ac.kr (K.J.Y.)
†These authors contributed equally to this work.

leading to have longer life span up to 6 months in a body (*17*–*20*). However, the current RF sensors require implantation and removal surgery, which increases the possibility of wounding and bacterial infection, presenting critical barriers for use.

Despite the considerable progress made by commercial CGMs, there remains a pressing need to develop user-friendly, minimally invasive CGMs. Researchers have explored the possibility of monitoring glucose levels in sweat and tears as a potential biofluid for noninvasive monitoring of blood glucose. While much research has been devoted to developing noninvasive wearable CGMs targeting sweat glucose, challenges such as requirement of hot and humid environments to obtain sufficient sweat quantity, and potential contamination from exogenous compounds including cosmetics, have hindered their commercial viability (*21*–*24*). In addition, the lens-type tear CGM has been studied; however, it presents inherent disadvantages, including low correlation between tear and blood glucose, a low concentration range, discomfort, and low biocompatibility (*25*–*27*). Therefore, a new class of CGM biosensors is needed for monitoring skin interstitial fluid (ISF) glucose, like commercial CGMs, in a user-friendly, minimally invasive way that overcomes the limitations of existing systems. Although there were slight differences in blood glucose and ISF glucose levels depending on the measurement sites, they clearly showed similar trends during continuous monitoring (*28*).

Recently, research on soft bioelectronics, such as wearable and implantable devices, has been actively conducted (*29*–*35*). These devices, which use biocompatible materials, are being studied for applications in the field of human health, in many forms, including diagnosis, treatment, physiological research, and clinical trials. Despite the inconvenience of their invasive nature, implantable devices can offer broad suggestions for health care. Bioresorbable devices are a promising approach to a more convenient and biocompatible use of this technology. Bioresorbable or transient devices dissolve or disappear in the human body without any harm because of the chemical properties of their materials. Moreover, because of the elimination of the need for a second surgery to remove the devices from the body, thus minimizing the risk of inflammation with inherent device in the body in the long term, these devices reduce surgical costs and the psychological burden of patients. Bioresorbable devices offer another avenue for the application of biomedical devices, and research on the development of various sensors is currently under way (*36*–*41*). Despite these advantages and wide applications, bioresorbable devices for CGM have not been reported.

Microneedle-type devices are other potential candidates for the monitoring of glucose levels in the body, as they are easy-to-use, easy-to-access, light, and thin micro-sized devices, which render them minimally invasive (*42*–*47*). The microneedle can be manufactured by adjusting its length, shape, density, etc. and is inserted at a shallower depth than the location of the subcutaneous pain point, thus serving its function without pain, discomfort, or injury to the skin. In addition, unlike the conventional skin-attached wearable devices, devices containing micro-sized needles are fixed to the skin; thus, they operate stably without falling off during activities. Because of their advantages, microneedles have been proposed as a previously underutilized class of tools that can be used not only for skin care, drug loading, and delivery but also for monitoring glucose. Microneedles have been considered as a tool for ISF extraction and a sensor platform for the third-generation CGM systems, suggesting an attractive alternative to the traditional lancet diagnostic method. When the hollow microneedles penetrate the skin, they extract subcutaneous ISF and continuously supply it to in vitro glucose sensors, with minimization of pain and skin damage (*48*–*50*). However, their fabrication process is complicated and difficult. In addition, they are easily clogged because of their small hole, and there is a high risk of breakage; these drawbacks hamper their application in clinical practice. Solid microneedles that extract subcutaneous ISF represent another solution for CGM (*51*, *52*). After the penetration of solid microneedles into the skin, making holes on the skin, ISF can be obtained via suction. However, the method of punching holes into the skin using a solid microneedle with suctioning is difficult to use for CGM. A recent study that integrated microneedles with a wearable sensor demonstrated their potential for use in CGM, even if the system was only used for a few hours (*53*). Although hydrogel microneedles circumvent the risk of clogging, the extraction process is cumbersome and requires laboratory facilities. Moreover, for CGM, it loses its practicality because it must be combined with a microneedle that extracts ISF and a sensor that measures it in an on-chip or hand-held manner.

Here, we present a minimally invasive fluorescence-based bioresorbable microneedle array for CGM that overcame the limitations of the previous systems. This system yielded simple but strong results using a method of measuring the fluorescence intensity of microneedles by reversibly expressing it according to glucose concentration, without the use of enzymes or reagents. The microneedle sensor containing a glucose-responsive fluorescent monomer (GF-monomer) with a high glucose-response-recognition selectivity expressed fluorescence after binding to glucose contained in the ISF within the body. This on-demand glucose monitoring system was operated completely tether free, thus allowing measurement at any desired time while the patient moved freely, and traced the glucose measurement results of the conventional lancet diagnostic method. User-friendly home glucose-level self-diagnosis is possible by applying a wireless portable accessory and a mobile application with image processing technology. The ability of our home diagnostic system to successfully trace blood-glucose levels, even when measured from multiple angles, had the advantage of covering diverse users and environments. In addition, the biodegradable microneedle array sensor offers several advantages over previous research that used GF-monomer for glucose monitoring (*54*). It is easy to manufacture and use, and it is composed of biocompatible materials, ensuring its safety for the human body. Also, there was no need to removal, as it completely dissolves and is naturally absorbed by the body after use. This feature notable reduces the risk of infection and further enhances patient comfort and compliance, making our system a more promising solution for CGM.

RESULTS

Design, concept, and principle of the biodegradable microneedle glucose sensor

Figure 1A shows an image of CGM using a biodegradable microneedle sensor. After attaching the sensor to a measurable part of the human body, such as an arm, illumination of the microneedle sensor with light at a wavelength of 405 nm led to the absorption of the light and its fluorescent reemission at 490 nm. The blood-glucose concentration can be visually checked on the basis of its

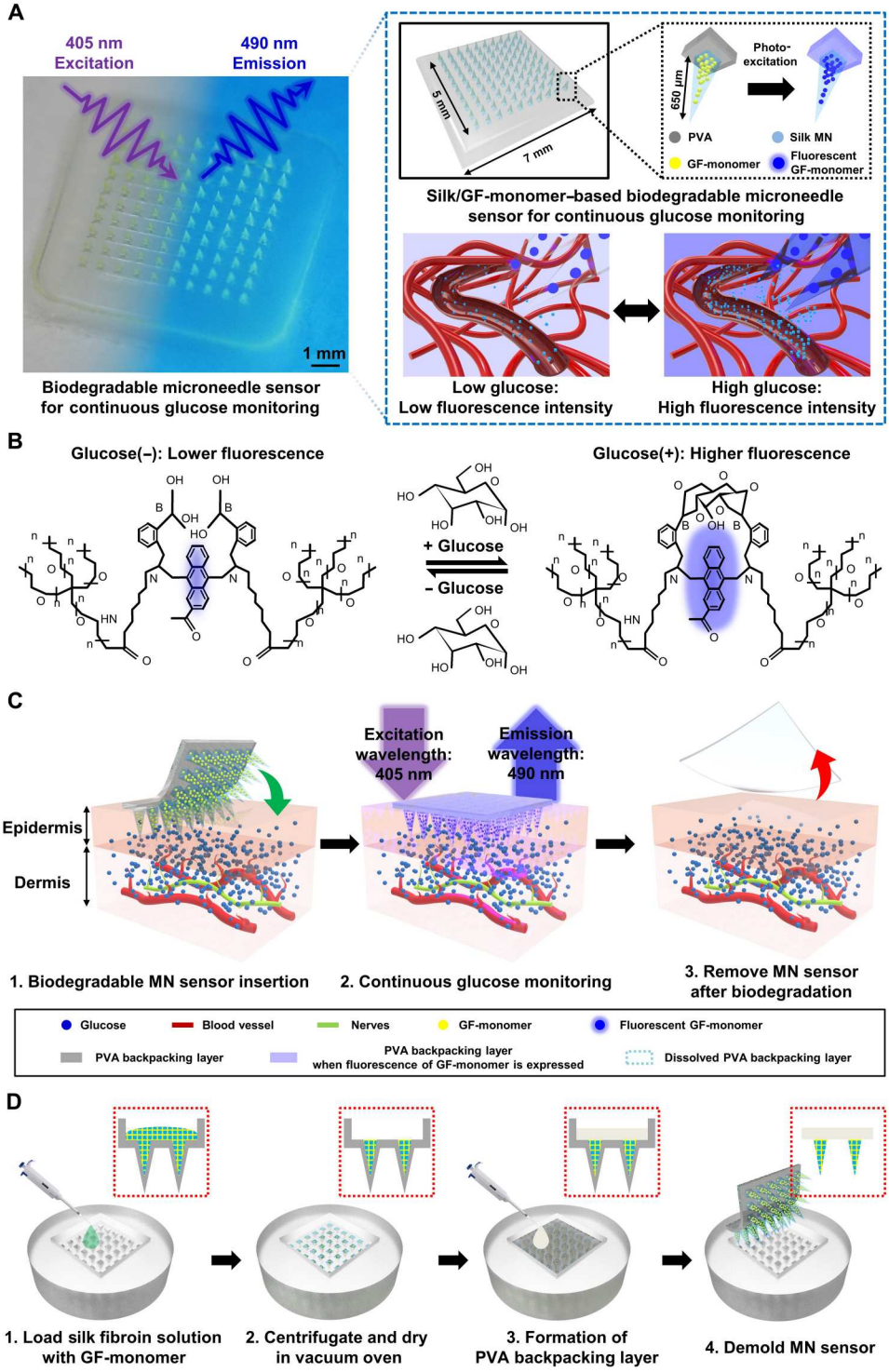

Fig. 1. Biodegradable microneedle array sensor for continuous glucose monitoring (CGM). (**A**) Image of the biodegradable microneedle glucose sensor (left) and illustrations of the arrays and single microneedles (right, top) and fluorescence expression of the sensor at low and high glucose (right, bottom). (**B**) In the presence of few glucose molecules, the fluorescence intensity of the anthracene moiety was low, whereas when many glucose molecules were present, the fluorescence intensity increased as the glucose molecules bound to arylboronic acid. (**C**) Schematic diagram of the continuous glucose measurement process using the biodegradable microneedle sensor. (**D**) Fabrication process of the biodegradable microneedle glucose sensor device, with side view. GF-monomer, glucose-responsive fluorescent monomer; PVA, poly vinyl alcohol.

fluorescence intensity on the sensor. The microneedle structure greatly improves light delivery more than four times compared to direct irradiation (*55*). The microneedle glucose sensor has a simple structure consisting of two layers: a needle layer made of silk, which is a well-known biodegradable material, containing a GF-monomer that fluoresces in response to blood-glucose level; and a poly vinyl alcohol (PVA) backpacking layer, to fix the needle and facilitate skin insertion. Silk is an amphiphilic compound, a naturally occurring protein polymer with hydrophobic and hydrophilicity characteristics and used in a variety of the drug delivery systems. Compared to hydrophobic materials, silk with hydrophilic properties increases the chance of contact with glucose in bodily fluids and has high sensitivity (fig. S1). Silk that has been bound with GF-monomer degrades after use; first, the hydrophilic block decomposes, and second, the immobilized hydrophobic crystal block migrates into the solution or biofluidic (*56*–*59*). PVA is also a biodegradable material that is safe for the human body (*60*, *61*). PVA has a lower Young′s modulus (707.9 MPa) than silk (14 to 36 GPa), which helps the microneedle sensor achieve conformal contact with the skin, and it exhibits favorable optical properties such as high optical transparency and transmittance (*60*–*68*). The size of the device is about 7 mm by 7 mm, and the length of the microneedle can be customized according to the target race, location, and skin condition of the patient. In this study, a 650-μm-sized microneedle was used in consideration of the average skin thickness of the arm (*69*, *70*). The fluorescence intensity of the microneedle sensor, which included a fluorescent substance, varied according to the glucose concentration in the ISF; i.e., our microneedles detected changes in blood glucose and exhibited a low fluorescence intensity at a low blood-glucose level and a high fluorescence intensity at a high blood-glucose level.

Figure 1B represents the mechanism of our sensors to sense glucose through fluorescence reactions: absorption and emission. The GF-monomer is composed of a diboronic acid moiety, which is a recognition site that binds to glucose, and an anthracene moiety that emits fluorescence. At a low glucose concentration, the fluorescence of the anthracene moiety is quenched by photo-induced electron transfer (PET). When glucose is bound to the diboronic acid moiety, a strong reaction between boron and nitrogen inhibits PET and the fluorescence of the anthracene moiety becomes stronger (fig. S2). The GF-monomer exhibits high mobility because of the increased opportunity of bonding with glucose molecules in body fluids and hydrophilic spacers. In other words, in the synthesis of the GF-monomer, polyethylene glycol (PEG; molecular weight = 3400) is used as spacers to enhance glucose capture, hydrophilicity, and biocompatibility. The anthracene and boronic acid moieties are strongly immobilized within these groups. The hydrophilicity and strong glucose affinity of GF-monomer make it a safe and effective glucose sensing platform. This design ensures a reliable and well-tolerated CGM system while minimizing potential adverse effects on the surrounding tissue (*54*, *71*–*73*). In addition, the diboronic acid moiety has a high glucose selectivity as its response recognition rate for glucose is 10 times stronger than that for other sugars (*17*–*19*). The principle of glucose sensing by the GF-monomer is presented in great detail in the previous study (*54*).

As shown in Fig. 1C, although the method and principle of operation of the biodegradable microneedle sensor for CGM is very simple and intuitive, it is a powerful system. The microneedle sensor, which is minimally invasive to the skin, penetrated a depth that was sufficient to indirectly measure glucose in blood vessels, thus allowing it to monitor blood glucose in the ISF. The fluorescence of the GF-monomer is expressed in microneedles with a wavelength of 490 nm using a 405-nm wavelength lamp. In this special material, with its unique ability, the brightness of the fluorescence of the microneedle varies according to the blood-glucose concentration in the body. Therefore, its users can monitor blood-glucose levels whenever they want while moving freely without external wireless communication equipment or connection lines. The fluorescence of the microneedle blood-glucose sensor can be checked using the naked eye; however, the use of an over 450-nm long-pass filter lens to block the light from the lamp would yield a more accurate blood-glucose result (fig. S3). The microneedle blood-glucose monitoring sensor completely dissolved and disappeared from the body after use, thus eliminating the need for additional surgery. In addition, biocompatible and biodegradable microneedles have high research and clinical value as they can be applied to drug loading and drug delivery, such as insulin, as well as blood-glucose monitoring. The biodegradable microneedle sensor enabled wireless CGM during free movement and minimized skin irritation because of its minimal invasiveness and absorption into the body, thus completely removing the risk of bacterial infection associated with surgery.

The existing continuous blood-glucose measurement equipment is bulky and heavy, which increases the patients′ discomfort and burden, and has disadvantages in that its manufacturing cost is very high and the price of the device is high. In contrast, the biodegradable microneedle sensor is extremely small, light, and thin, and the fabrication process is relatively easy and inexpensive. Figure 1D depicts the sequence of the process of fabrication of the biodegradable microneedle glucose sensor. A mixed solution of silk fibroin and GF-monomer was injected into a poly(dimethylsiloxane) (PDMS) microneedle mold, and vacuum was held in the desiccator to spread the solution evenly into the mold. After allowing the mixed solution to completely enter the microneedle through centrifugation, it was sufficiently dried in a vacuum oven. The PVA solution was then injected, to form the backpacking layer, and centrifugation was used to spread it evenly throughout the microneedle mold. After drying completely in a vacuum oven, the device was removed from the microneedle mold. Details on preparation and process of microneedle sensor in Materials and Methods. Because all materials constituting the microneedle sensor are protein- and polymer-based materials, care must be taken in the process so that they are not denatured at high temperatures. The biodegradable microneedle sensor can be formed into a desired shape and size using various microneedle molds. The microneedle mold manufacturing technology has been widely studied and commercialized; therefore, researchers can easily access it.

Characteristics and in vitro measurement of biodegradable glucose devices

A photographic image of the fabricated biodegradable microneedle sensor is provided in Fig. 2A. Silk fibroin was semitransparent, PVA was transparent, and the GF-monomer was yellow; thus, the microneedle sensor was a translucent device with a slightly yellow tint. Figure 2B presents an optical microscopy image acquired by magnifying the microneedles of the device. The length of the microneedle sensor manufactured and used in this study was 650 μm, and all 100 microneedles had the same length and shape. Figure 2C

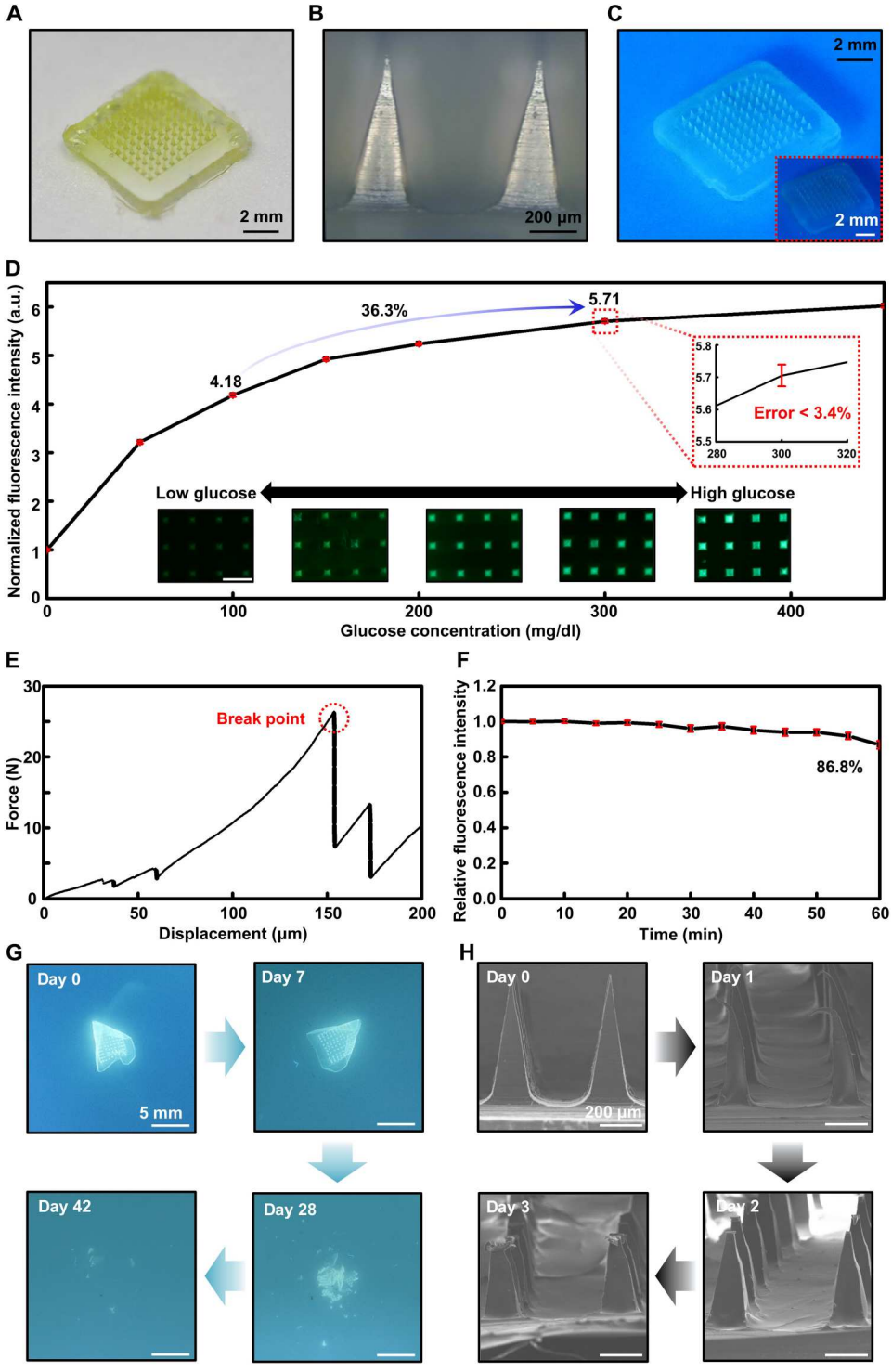

Fig. 2. Illustrations and in vitro performance of the biodegradable microneedle glucose sensor. (**A**) Optical image of a biodegradable microneedle array glucose sensor device. (**B**) Scanning electron microscopy (SEM) image of a microneedle. (**C**) Photographs of the fluorescence-expressing microneedle glucose sensor array with and without (inset) a long-pass filter. (**D**) In vitro characteristic results and optical microscope images of the microneedle glucose sensor. Fluorescent images of the microneedle sensor array (inset; scale bar, 500 μm). a.u., arbitrary units. (**E**) Mechanical performance of the biodegradable microneedle sensor. (**F**) Photobleaching properties of the silk microneedle sensor including a glucose-responsive fluorescent monomer (GF-monomer). (**G**) Images showing the time sequence of the dissolution of the sensor by immersion in phosphate-buffered saline (60°C; pH, 4.01) for days 0, 7, 28, and 42. (**H**) SEM images of the dissolved microneedle after insertion into a gelatin skin model.

provides an image that was acquired using a long-pass filter after expressing the fluorescence of the microneedle sensor by applying light using a lamp. The inset of Fig. 2C shows that, although the biodegradable microneedle sensor can be checked using the naked eye, the use of a filter that blocks light below a wavelength of 460 nm blocks light of 405-nm wavelength, which is the light of the lamp used for excitation; therefore, only the desired fluorescence result can be obtained, yielding more accurate and intuitive results.

We confirmed the performance of the biodegradable microneedle glucose sensor through in vitro testing and established the applicability of the biocompatible and bioresorbable polymer material–based device to the human body for CGM. Before fabrication of the microneedle shaped device, a silk film containing GF-monomer was prepared to verify the fluorescence response to glucose (fig. S4). Figure 2D confirms the measurement capability of the microneedle blood-glucose sensor in vitro. Glucose measurements were carried out under conditions ranging from 50 mg/dl, a hypoglycemic level, to 450 mg/dl, a level above hyperglycemia. Sequence of images for the microneedles at each concentration are shown collectively. The microneedle blood-glucose sensor containing the GF-monomer exhibited a greater change in the hypoglycemia range than in the hyperglycemia range. When the glucose concentration increased from 100 mg/dl, which is a general low blood-glucose value, to 300 mg/dl, which is a high blood-glucose value, the fluorescence intensity of the biodegradable microneedle sensor increased by about 36.3%. Moreover, the inset of this figure shows that, to check the reliability of the device, we performed 10 measurements for each range, with a maximum error of about 3.4%, which is negligible for monitoring changes in human blood glucose. To successfully monitor glucose levels in the ISF of the dermis, microneedle array sensors must be able to penetrate the stratum corneum of the skin without breaking. Figure 2E and fig. S5 report the mechanical properties of the biodegradable microneedle glucose sensor. We verified the average mechanical property of the microneedle using a compression test, which confirmed that the minimum force for fracture per single patch was about 13.4 N. The fracture force of our single microneedle was determined to be 0.795 N, which sufficiently surpasses the minimum force of 0.045 N required for penetrating the stratum corneum (fig. S6). This result supports the conclusion that the microneedle can penetrate the epidermis and be properly inserted into the body as necessary (*69*, *70*, *74*–*76*). In addition, the microneedle insertion test on pig skin confirmed that our device had sufficient mechanical strength (fig. S7).

We tested the effect of photobleaching the biodegradable microneedle sensor developed in this study (Fig. 2F). Excited light (405 nm, 60 W) was continuously applied to the microneedle containing a fluorescent material; after 60 min, it decreased to about 86.8%. To minimize the effect of the photobleaching of the microneedle sensor during CGM, a method for applying light during the measurement exclusively can be used. For example, if the microneedle fluorescence measurement is performed 10 times per day using an exposure of 1 s, then photobleaching would be about 1% after 1 month, which far exceeds the target use time of biodegradable microneedle sensors (*54*).

The biodegradable microneedle blood-glucose sensor dissolved in the body after a certain period of use and did not need to be removed (*46*). Silk fibroin, which was the main component of the microneedle sensor, resorbed slowly in the body, and the GF-monomer was separated from the microneedle. The degraded silk and GF-monomer were transferred to the biofluid and completely dissolved to exit the body. Figure 2G depicts the disintegration and dissolution of the blood-glucose measurement device in phosphate-buffered saline (PBS) (60°C; pH, 4.01). After the PVA backpacking layer was dissolved, the microneedle arrays composed of silk fibroin were also dissolved. We performed a degradation test using a gelatin skin model to confirm the melting degree of the microneedle sensor embedded in the skin. Figure S8 shows that, after the device was inserted into the gelatin skin model, the fluorescence material was separated and gradually escaped as the microneedle dissolved. Figure 2H shows the corresponding scanning electron microscopy (SEM) image, which was used to verify the melting degree of the microneedle on each day during the use of the sensor. The 650-μm-long microneedles melted and shrank to a size of 400 to 450 μm on the third day after their insertion.

Biocompatibility assessment and biodistribution investigation of GF-monomer–loaded microneedles

A needle insertion test was performed to verify the skin-penetration ability of our microneedles using hematoxylin and eosin staining of mouse skin. The skin was cross-sectioned and stained after the microneedle insertion and immediate removal. As shown in Fig. 3A, skin penetration by a needle of about 400 μm was observed in the cross section of the skin tissue. To assess not only the skin-penetration ability but also the skin regeneration and recovery after the insertion of the microneedle, the mouse skin cross section was checked 3 days after the embedding of the microneedle into the mouse skin and 7 days after its removal, i.e., day 10. The skin cross section at 3 days after insertion revealed needle penetration with a slightly shallower depth than that obtained via immediate removal after insertion, whereas the cross section at 7 days after removal showed afterimages of the needle with a shallow depth of about 100 μm because of skin regeneration. Through the top viewed optical image, we confirmed that the mouse skin recovered to its original state without injury after removing the microneedle sensor (fig. S9).

To assess the biocompatibility of our microneedle patch, we examined the distribution of activated macrophages via immunofluorescence staining with an anti-CD206 antibody, for selective identification of M2 macrophages; an anti-CD68 antibody, for staining whole activated macrophages; and 4′,6-diamidino-2-phenylindole (DAPI), for counterstaining cell nuclei. After embedding the microneedle in the mouse skin, it was fixed with formalin, embedded in paraffin, and sectioned. Total macrophages (red) and M2 macrophages (green) are visualized in Fig. 3B. On day 1, total and M2 macrophages were observed as a result of microneedle infiltration; moreover, on days 7 and 14, it was confirmed that macrophages decreased remarkably over time, thus assuring the biocompatibility of our microneedle and recoverability after insertion.

A pharmacokinetics analysis using an in vivo imaging system (IVIS) was conducted to confirm the safe excretion of the GF-monomer from the body after its spread through the microneedles. On the basis of the principle that the IVIS detects fluorescent substances in the body, biodistribution of the GF-monomer with an emission length of 490 nm was observed. According to a previous study that reported that monomers with a size of 5 nm or less are

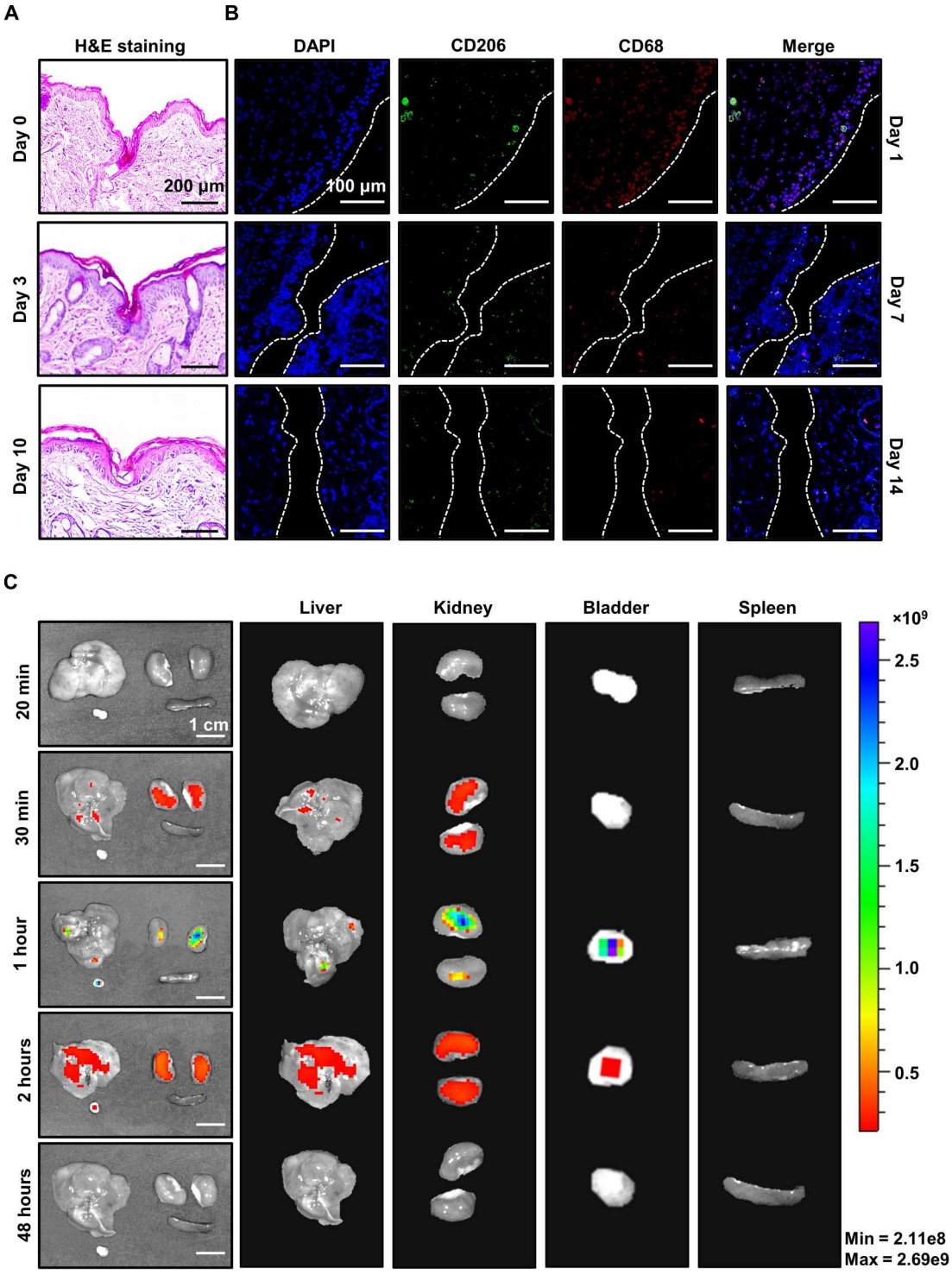

Fig. 3. Investigation of the biocompatibility and needle insertion of the biodegradable microneedle sensor through staining and imaging. (**A**) H&E staining (right) of the mouse skin after microneedle insertion (at day 0, day 3, and day 10; scale bar, 200 μm). (**B**) Immunofluorescence from 4′,6-diamidino-2-phenylindole (DAPI), CD206, and CD68 staining of the mouse skin after device-insertion surgery detected at day 1, day 7, and day 14. The green and red fluorescence are macrophages: green (M2), red (total macrophages). (**C**) Investigation of the biodistribution in the main urinary organs using an in vivo imaging system (IVIS) after intraperitoneal injection of the glucose-responsive fluorescent monomer (GF-monomer) solution.

excreted in the urine without accumulating in the lymph nodes, the extraction of the excretory system for fluorescence expression was selected. The GF-monomer was diluted in saline solution at a ratio of 2% (w/v), and 150 μl of the solution was subcutaneously injected into mice.

The mice were euthanized and the liver, kidney, bladder, and spleen were collected in 20 min, 30 min, 1 hour, 2 hours, and 48 hours after injection, respectively. As shown in Fig. 3C and fig. S10, the fluorescence of the monomer was concentrated and distributed in the liver up to 10 to 30 min after dosing and was slightly expressed in the kidneys; in contrast, after 2 hours, it was only distributed in the bladder, and after 24 hours, it had been eliminated from all organs. The biodistribution of the GF-monomer revealed that it moved from the liver to the bladder and was excreted through urine with time.

In vivo continuous blood-glucose measurement using the biodegradable microneedle sensor

To confirm that the biodegradable microneedle blood-glucose sensor can continuously measure blood glucose in living tissues, we performed an in vivo experiment using mice. To clearly capture the expression of fluorescence in the microneedle sensor during the experiment, we selected nude mice. Figure 4A shows the overall setup of the experiment and a fluorescence photograph, as well as a postprocessed photograph that was used to check the fluorescence intensity using ImageJ (Figure 4B and C). We selected the back of the mouse as the application location, as all biodegradable microneedle blood-glucose sensor arrays could be sufficiently inserted and operated stably over a long period in this area.

We injected glucose solutions into three mice and induced hyperglycemic conditions that were similar to those of real patients with diabetes (*77*, *78*). After the blood-glucose level reached the maximum and became saturated, we lowered the blood glucose to the normal and hypoglycemic range by injecting insulin. Although there was a slight difference between mice, the values varied from hypoglycemia of about 40 mg/dl to hyperglycemia of about 280 mg/dl. Concomitantly, the blood-glucose measurement was carried out on the tail of the mouse using a commercial sensor. In all procedures, the biodegradable microneedle blood-glucose sensor successfully monitored the mouse blood-glucose level and completely traced the result of enzyme detection–type blood-glucose measurement through blood collection (*8*, *79*). The measurement was carried out over a period of 2 to 3 hours, during which the microneedle sensor performed CGM completely. The result of our device lagged by about 20 min behind the change in blood-glucose concentration (Figure 4D and fig. S11). The time delay of the biodegradable microneedle blood-glucose sensor, which measures the change in the glucose concentration in the subcutaneous ISF, was caused by the time lag between the change in blood-glucose concentration and that of interstitial glucose. From 100 to 250 mg/dl, which is the normal blood-glucose range, mice #1, #2, and #3 showed a variation of 36.6, 30.3, and 31.9%, respectively, which was a very good and sensitive change in fluorescence brightness. As the biodegradable microneedle blood-glucose sensor dissolved in the body, the absolute amount of fluorescent material was decreased; thus, the sensitivity decreased gradually. Figure 4E reveals that the change in fluorescence intensity decreased to 27.3% in the range of 100 to 250 mg/dl at 1 day after device insertion and decreased to 18.4% after 2 days (Fig. 4F). After 3 days, the biodegradable microneedle blood-glucose sensor had completely lost its performance and could not trace blood glucose properly (Fig. 4G). The microneedle blood-glucose sensor can be applied not only to a specific part of the mouse in the laboratory but also to humans by adjusting its size, length, and number of arrays via customization of the mold. The user can move freely during and after the application of the biodegradable microneedle blood-glucose sensor and can live normally without any side effects after use (movie S1).

User-friendly home diagnosis system with a smartphone application and attachable ultraviolet-delivering lamp

To demonstrate the actual usability of our device in daily life, we developed a user-friendly home diagnosis system that enabled CGM in a freely moving state using biodegradable microneedle sensors and a smartphone (Fig. 5A and movies S2 to S4). An external accessory device attachable to a camera of a smartphone provided a 405-nm light-emitting diode (LED) array as a light source for activating the fluorescence of GF-monomers and a 450-nm optical long-pass filter for removing unwanted 405-nm light that could be received by the camera lens (fig. S12). The custom-developed smartphone application allowed users to intuitively perform various functions, such as taking photos, cropping images, analyzing image data to measure glucose levels, and plotting the measured data, so that they could easily recognize their state.

After the filtered optical image was acquired through the mobile application, the user cropped the picture to remove the unnecessary part (other than the sensor). The image filtering process was detailed in Materials and Methods. Fluorescent light with a wavelength of 490 nm had a relatively large green pixel value in the image; thus, it was possible to filter the fluorescent pixels from the surrounding pixels. The filtered pixels exhibiting fluorescence contained information about both fluorescent reactions of the GF-monomers and ambient brightness, whereas the remaining pixels contained information about the ambient brightness exclusively. By subtracting the average of the surrounding pixel values from the fluorescent pixels, fluorescence image data were obtained. The glucose level was lastly determined on the basis of the average pixel values of the fluorescence image data. The measured data were automatically recorded in the local file system and plotted on a graph, to be easily checked by the users and help them manage their blood sugar levels.

The feasibility of our home diagnosis system was confirmed by performing in vivo experiments using rodent models. Because the fluorescence data are affected by various factors, such as camera angles or the distance between the camera and the sensor, the minimization of data variability is required. To address this issue, users can calibrate the fluorescence image data via repeated measurements from different angles (Fig. 5B). Image data from multiple angles are averaged to improve data reliability and reduce fluctuations. As shown in Fig. 5C, it was verified that the calibrated data repeatedly measured by our home diagnosis system (four times) tracked blood-glucose levels with a 15- to 20-min time delay.

DISCUSSION

Continuous monitoring of glucose in patients with diabetes is essential for the management of diabetes, a fatal disease with a high risk of complications and steadily increasing number worldwide

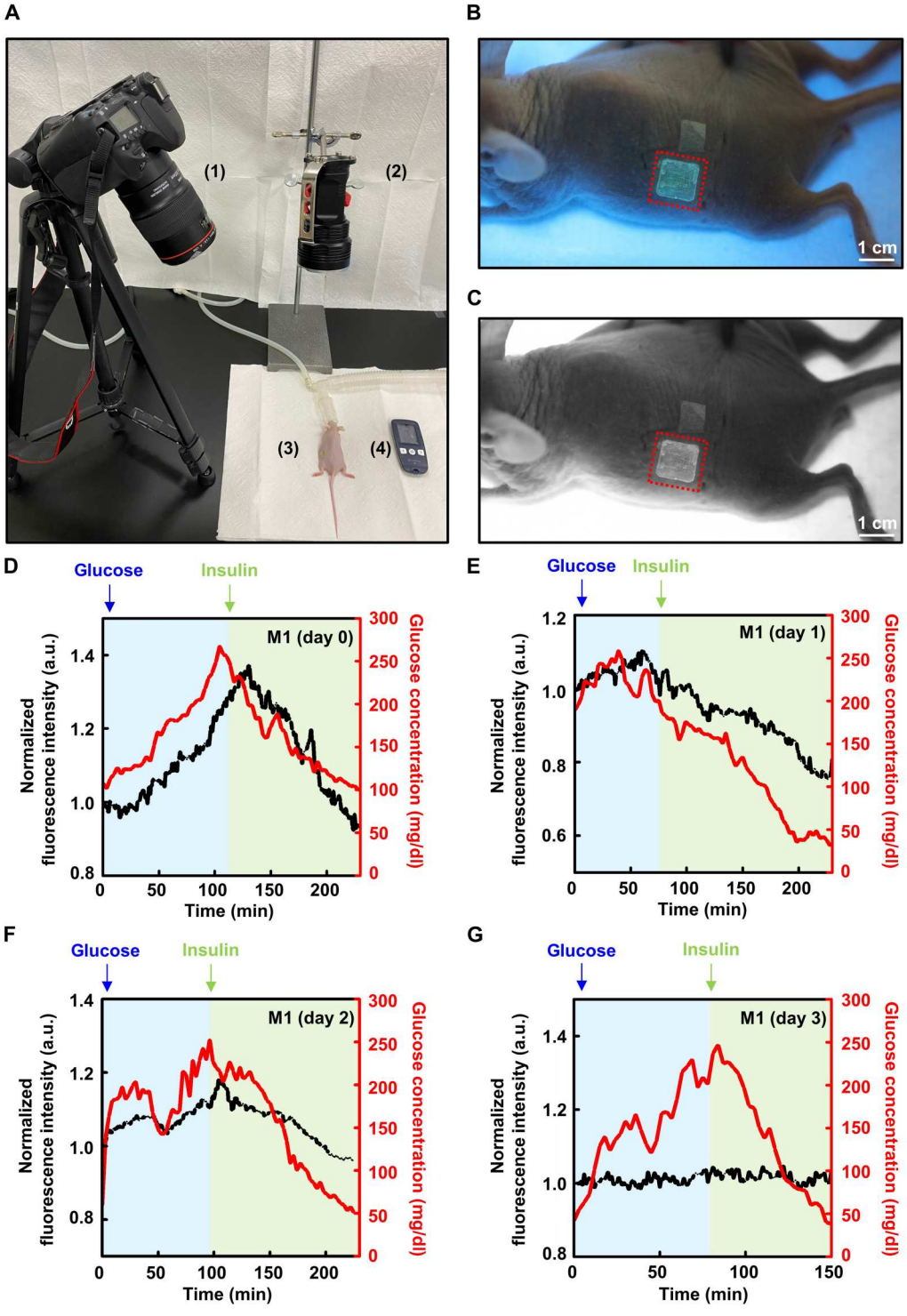

Fig. 4. In vivo continuous glucose monitoring (CGM) using a biodegradable microneedle sensor. (**A**) In vivo setup image of the continuous glucose measurement with a mouse model: (1) digital camera with a long-pass filter lens, (2) lamp, (3) mouse with an inserted microneedle glucose sensor, and (4) glucometer. (**B**) Fluorescence photograph of the microneedle sensor attached to the mouse model. A 405-nm lamp and a 450-nm long-pass filter were used. (**C**) Image analyzed using ImageJ. (**D** to **G**) In vivo results obtained using a biodegradable microneedle glucose sensor and a glucometer (black, relative fluorescence intensity; red, glucose concentration measured by the glucometer). The CGM results were measured on day 0, day 1, day 2, and day 3. a.u., arbitrary units.

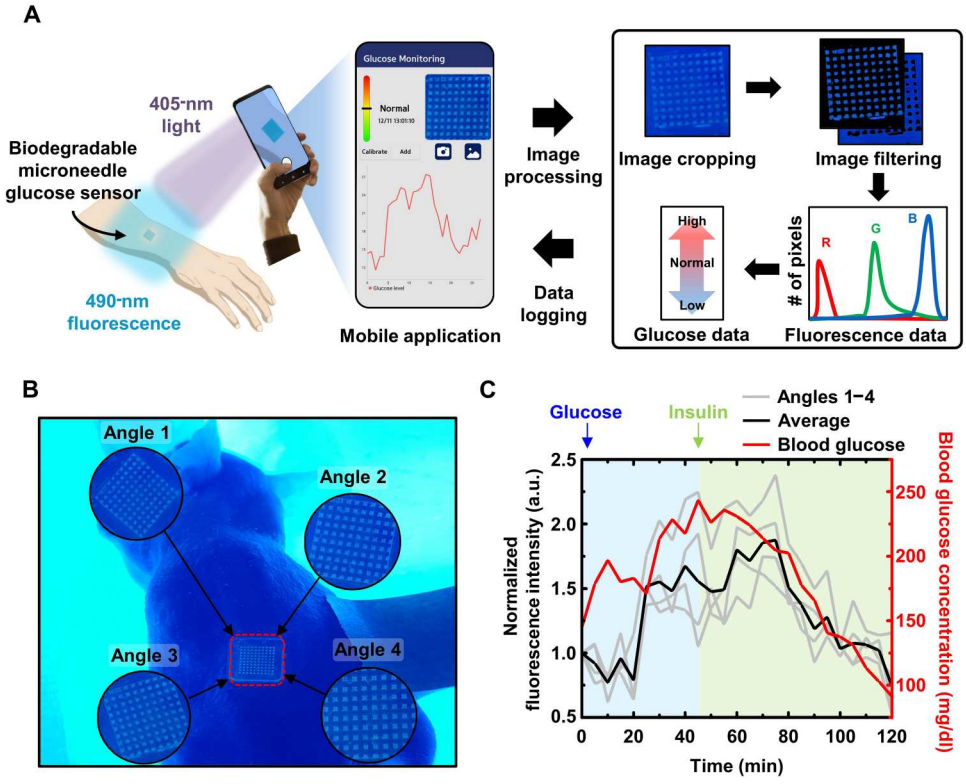

Fig. 5. Operation of the user-friendly home diagnosis system. (**A**) Overview of the home diagnosis glucose system. (**B** and **C**) Fluorescence images and graphs of the results of the microneedle glucose sensor obtained using the mobile application at various angles (black, mean value of the fluorescence intensity results from four angles; gray, fluorescence intensity results from four angles; red, glucose concentration measured by the glucometer). a.u., arbitrary units.

(*80*). The biodegradable microneedle–based fluorescent sensor that continuously monitored glucose level in real time without pain via a procedure that was minimally invasive to the skin is proposed. The sensor system, which was composed of biocompatible materials, wirelessly measured glucose in a freely moving environment and was completely biodegradable and discharged from the body without the need for its removal after use. We confirmed the detection of fluorescence intensity changes with high precision at various glucose concentrations including all human blood-glucose ranges in vitro and successfully monitored glucose levels over several consecutive days; moreover, we tracked blood-glucose measurements in vivo in the mouse. This suggested the potential application of the biodegradable microneedle–based glucose-responsive fluorescent sensor for long-term CGM. The home diagnosis system using a smartphone allowed users to check blood sugar changes easily and autonomously and to plan diagnosis and treatment, thus improving patient health and quality of life. This state-of-the-art home diagnostic device can sufficiently track the glucose level even when measuring from any angle under the various patient's situation. The microneedle sensor can be adjusted to a desired shape, size, and number of arrays depending on the mold, which has the advantage of being able to cover all aspects of the diversity of use of these devices, such as race or application location. By increasing the degradation time of the microneedle sensor through the proper application of biodegradable materials and manufacturing process and reducing the photobleaching of GF-monomers through minimal exposure, it is possible to develop a CGM device with a life span of several months or more. The proposed groundbreaking measurement system overcame the disadvantages of previous methods, such as discomfort, pain, wounding, surgery, high cost, complex processes, inability to perform CGM, and short usage time. Therefore, this system completely replaced conventional blood-glucose measurement method, such as the lancet approach, so that patients with diabetes can conveniently and accurately prevent the disease, hypoglycemia, or hyperglycemia. In addition, the biodegradable microneedle array device developed in this study can load drugs such as insulin; thus, there is a high possibility of expansion of this device into a next-generation fusion bio system that can simultaneously monitor and treat glucose-related diseases.

MATERIALS AND METHODS

Fabrication of the biodegradable microneedle glucose sensor

PDMS female molds for square pyramid–shaped microneedles with a height of 650 μm, a base of 200 μm by 200 μm, and a pitch of 500 μm in 10 × 10 arrays were purchased from Micropoint. The microneedle molds included a 7 mm by 7 mm by 1 mm (width by length by height) pedestal box, to support the microneedle array (fig. S13). Biodegradable microneedles for glucose sensing were sequentially manufactured as follows. First, 10 ml of a 5% (w/v) of a silk fibroin dispersion aqueous solution purchased from Sigma-Aldrich and the prepared glucose monomer powder were mixed

at a ratio of 10% (w/v) through gentle agitation, to prevent the formation of a colloid of silk fibroin. Then, 20 μl of the mixed aqueous solution was transferred to the prepared mold through a micropipette and loaded onto the mold via centrifugation at 4000 rpm for 20 min (VS-400, VISION SCIENCE Co., Ltd.). Subsequently, the microneedle was completely dried (2 hours) in a vacuum oven at 50°C under 1 atm (SH-VDO-08NG, SH SCIENTIFIC). To prepare the backpacking to support the microneedle array, a PVA powder purchased from Sigma-Aldrich was dissolved in deionized water at 30% (w/v) through agitation, to obtain a mixed aqueous solution. Next, 60 μl of the sucrose PVA aqueous solution was transferred onto the mold loaded with silk and glucose monomers using a micropipette and dispersed onto the mold via centrifugation at 4000 rpm for 60 min. After completely drying of the microneedle (2 hours) in a vacuum oven at 55°C under 1 atm, it was separated from the mold to obtain a biodegradable silk microneedle for glucose sensing. The manufactured microneedle glucose sensor array device has a height of 650 μm and a weight of 65 mg.

In vitro test

To confirm the glucose sensitivity of the microneedles, glucose aqueous solutions at concentrations of 0, 50, 100, 150, 200, 300, and 450 mg/dl were prepared. After loading the prepared microneedles onto a PDMS resolver mold with a size of 7 mm by 7 mm by 1 mm, 150 μl of the prepared glucose aqueous solution was added. A long-pass filtering lens (Edmond Optics, >450 nm) was attached to an optical microscope (Olympus company), and a light source with a wavelength of 405 nm (CREE company) was used for irradiation at a power of 230 $\mu W/mm^2$ for 1 s. The measured images were analyzed by an ImageJ program.

Mechanical test

To verify the penetration ability of the microneedles, a mechanical test with correlation with the compression force was performed (Instron Universal Testing Systems, 5966) (fig. S14). In the programming step of the pressing material characteristics of the machine, the needle shape was specified as a square pyramid. A single microneedle patch loading 100 microneedles (10 × 10) was placed on the rigid base of the station with the needles facing upward. The steel load cell compressed the patch horizontally at a constant speed of 1 mm/min. The initial distance of measurement was calculated when the load cell was about 1.5 mm away from the backpacking layer of the microneedle patch, with values being recorded from the moment at which the load cell started to touch the tip of the microneedle.

Photobleaching test

The prepared microneedles were continuously irradiated with a light source with a wavelength of 405 nm (CREE company) at a power of 230 $\mu W/mm^2$ for 60 min and then photographed through the long-pass filtering lens (Edmond Optics, >450 nm), which was placed in front of the lens of the camera (Cannon EOS 80D, EF100mm F2.8 L IS MACRO USM Lens). The images were analyzed for photobleaching using the ImageJ program.

Degradation test

The biodegradable microneedles were carefully inserted into the 10 weight % gelatin (Sigma-Aldrich), which was prepared on the basis of a glucose aqueous solution (100 mg/dl). A light source with a wavelength of 405 nm (CREE company) was used for irradiation at a power of 230 $\mu W/mm^2$ for 1 s; subsequently, images were acquired every 0, 1, 2, and 3 days through a camera (Cannon EOS 80D, EF100mm F2.8 L IS MACRO USM Lens) equipped with a long-pass filtering lens (Edmond Optics, >450 nm) in front of the camera lens. Next, the microneedle sensor was sufficiently dried in a desiccator at 27°C and then photographed on a field emission scanning electron microscope (IT-500HR from JEOL).

Animals

Male SKH-1 mice with 6 to 8 weeks′ age were purchased from Orient Bio (Korea). The nonpedigreed hairless strain of SKH-1 mice were chosen for in vivo experiments to minimize interference with the fluorescence expression of the device. All in vivo experiments were conducted with following the regulations of the Institutional Animal Care and Use Committee of the Korea Institute of Science and Technology (study approval number: KIST-5088-2022-05-081).

Biocompatibility test

For biocompatibility test, general protocol of immunofluorescence was followed. The microneedle array was sterilized with ethylene oxide gas and inserted subcutaneously into the mouse (SKH-1, male, 7 weeks). After explanation of the device at 1, 7, and 14 days, the surrounding tissue was fixed for 24 hours with paraformaldehyde and dehydrated. Dehydrated tissues were embedded in paraffin blocks and sectioned at 5-μm thickness using microtome (RM2255, Leica). For immunofluorescence staining, the paraffin sections were rehydrated with xylene and ethanol and treated with protease for antigen exposure. After antigen retrieval, bovine serum albumin blocker was treated for blocking other reagents. Next, a mouse anti-CD68 antibody (sc-20060; Santa Cruz Biotechnology) diluted at 1:100 was incubated in room temperature for 2 hours. After washing in diluted water, a rabbit anti-CD206 antibody (sc-376232; Santa Cruz Biotechnology) diluted 1:100 was incubated in room temperature for 2 hours. After washing off in PBS, the sections were counterstained with DAPI.

In vivo optical imaging system (IVIS)

GF-monomers were diluted in saline solution at a ratio of 2% (w/v), and 150 μl of the solution was injected subcutaneously into the mouse (SKH-1, male, 7 weeks). After injection, a mouse was euthanized for each time point and the urinary system (liver, kidneys, spleen, and bladder) was extracted and washed in PBS. The organs were aligned on the observation pad of the IVIS system. Considering the excitation and emission wavelength bands of the GF-monomer, fluorescent light in the excitation wavelength band of 450 nm and the emission wavelength band of 490 nm was observed.

In vivo test

The in vivo test for glucose tracking was performed using male hairless mouse (SKH-1, 6 to 8 weeks of age). The mice fasted for 18 hours to acquire a stable initial glucose level. For the modulation of glucose levels in the mouse, a 50% glucose solution (G8644, Sigma) was injected intraperitoneally at 5 ml/kg. To temporarily lower the glucose level, insulin (Novolin R, Novo Nordisk Pharma Ltd) was diluted in a 0.9% NaCl solution, and 0.5 U/kg was injected after the glucose level increased to a maximum.

Blood collected from the tail of a mouse via a cut that was performed using a laser blade was measured every 3 min through a blood collection–type blood-glucose meter (SD CodeFree Blood Glucose Monitoring System, 01GC110). We repeatedly turned the lamp on and off at 1-min intervals and took fluorescent photos of the microneedle sensor using a camera (Cannon EOS 80D, EF100mm F2.8 L IS MACRO USM Lens) equipped with a long-pass filter (Edmond Optics, >450 nm).

Smartphone application for user interface and data analysis

The smartphone application used as a user interface was built in Android Studio with the Kotlin programming language. The user was able to use the camera within the application to take fluorescence pictures or import and analyze pretaken pictures. For cropping the taken and imported images, the Croppy library (Apache License 2.0) was used. After cropping the image, it was converted to a three-channel RGB bitmap and then filtered, to isolate the fluorescent pixels. Because fluorescent light has a wavelength of 490 nm, the green pixel value was higher than that of other regions that did not exhibit fluorescence. The image processing function was used to examine each pixel, to check whether the green pixel value g and the blue pixel value b satisfied the following condition

$$g \geq \alpha \cdot b$$

where α is a constant value between 0 and 1. If the pixel satisfied this condition, then it was classified into the fluorescent pixel group. In our application, the value of α was set to 0.35 through several tests (fig. S15). The filtered fluorescent pixels and the remaining pixels were saved to separate bitmaps. The average pixel value of the fluorescent pixel group was subtracted from that of the remaining pixel group, to remove the noise caused by the ambient light. To present a graph of processed fluorescence data indicating the glucose levels on the user interface, a line chart of the MPAndroidChart library (Apache License 2.0) was used.

Printed circuit board module as a UV light source in the home diagnosis system

The UV light source for the home diagnosis system was implemented by designing a printed circuit board module that could be attached to the back of a smartphone. The light-delivering part consisted of eight LEDs (VLMU3100-GS08) with a wavelength of 405 nm. The module was powered by an external battery, and the supply voltage applied to each anode of the LEDs was regulated by a boost converter chip (SC121ULTRT), to maintain it at 3.6 V. The operation of the LED array was controlled by an eight-channel LED driver (ALED8102SXTTR). The module had a 6-mm-diameter hole that was open to the camera lens, and an optical 450-nm long-pass filter film was attached to this part, to receive fluorescent light more effectively.

Supplementary Materials

This PDF file includes:
Supplementary Text
Figs. S1 to S15
Legends for movies S1 to S4

Other Supplementary Material for this manuscript includes the following:
Movies S1 to S4

View/request a protocol for this paper from *Bio-protocol*.

REFERENCES AND NOTES

1. H. Sun, P. Saeedi, S. Karuranga, M. Pinkepank, K. Ogurtsova, B. B. Duncan, C. Stein, A. Basit, J. C. N. Chan, J. C. Mbanya, M. E. Pavkov, A. Ramachandaran, S. H. Wild, S. James, W. H. Herman, P. Zhang, C. Bommer, S. Kuo, E. J. Boyko, D. J. Magliano, IDF Diabetes Atlas: Global, regional and country-level diabetes prevalence estimates for 2021 and projections for 2045. *Diabetes Res. Clin. Pract.* **183**, 109119 (2022).
2. A. H. Heald, M. Stedman, M. Davies, M. Livingston, R. Alshames, M. Lunt, G. Rayman, R. Gadsby, Estimating life years lost to diabetes: outcomes from analysis of National Diabetes Audit and Office of National Statistics data. *Cardiovasc. Endocrinol. Metab.* **9**, 183–185 (2020).
3. Y. Cui, L. Zhang, M. Zhang, X. Yang, L. Zhang, J. Kuang, G. Zhang, Q. Liu, H. Guo, Q. Meng, Prevalence and causes of low vision and blindness in a Chinese population with type 2 diabetes: the Dongguan Eye Study. *Sci. Rep.* **7**, 11195 (2017).
4. Y. Ohkubo, H. Kishikawa, E. Araki, T. Miyata, S. Isami, S. Motoyoshi, Y. Kojima, N. Furuyoshi, M. Shichiri, Intensive insulin therapy prevents the progression of diabetic microvascular complications in Japanese patients with non-insulin-dependent diabetes mellitus: a randomized prospective 6-year study. *Diabetes Res. Clin. Pract.* **28**, 103–117 (1995).
5. O. Veiseh, B. C. Tang, K. A. Whitehead, D. G. Anderson, R. Langer, Managing diabetes with nanomedicine: Challenges and opportunities. *Nat. Rev. Drug Discov.* **14**, 45–57 (2015).
6. K. M. Bratlie, R. L. York, M. A. Invernale, R. Langer, D. G. Anderson, Materials for diabetes therapeutics. *Adv. Healthc. Mater.* **1**, 267–284 (2012).
7. M. Stumvoll, B. J. Goldstein, T. W. van Haeften, Type 2 diabetes: principles of pathogenesis and therapy. *Lancet* **365**, 1333–1346 (2005).
8. W. T. Golde, P. Gollobin, L. L. Rodriguez, A rapid, simple, and humane method for submandibular bleeding of mice using a lancet. *Lab Anim.* **34**, 39–43 (2005).
9. Y. J. Heo, H. Shibata, T. Okitsu, T. Kawanishi, S. Takeuchi, Long-term in vivo glucose monitoring using fluorescent hydrogel fibers. *Proc. Natl. Acad. Sci. U.S.A.* **108**, 13399–13403 (2011).
10. M. Park, Y. J. Heo, Biosensing technologies for chronic diseases. *Biochip J.* **15**, 1–13 (2021).
11. L. Lei, C. Zhao, X. Zhu, S. Yuan, X. Dong, Y. Zuo, H. Liu, Nonenzymatic electrochemical sensor for wearable interstitial fluid glucose monitoring. *Electroanalysis* **34**, 415–422 (2022).
12. Y. J. Heo, S.-H. Kim, Toward long-term implantable glucose biosensors for clinical use. *Appl. Sci.* **9**, 2158 (2019).
13. R. Wilson, A. P. F. Turner, Glucose oxidase: An ideal enzyme. *Biosens. Bioelectron.* **7**, 165–185 (1992).
14. G. P. Forlenza, T. Kushner, L. H. Messer, R. P. Wadwa, S. Sankaranarayanan, Factory-calibrated continuous glucose monitoring: How and why it works, and the dangers of reuse beyond approved duration of wear. *Diabetes Technol. Ther.* **21**, 222–229 (2019).
15. S. V. Edelman, N. B. Argento, J. Pettus, I. B. Hirsch, Clinical implications of real-time and intermittently scanned continuous glucose monitoring. *Diabetes Care* **41**, 2265–2274 (2018).
16. Z. Pu, R. Wang, J. Wu, H. Yu, K. Xu, D. Li, A flexible electrochemical glucose sensor with composite nanostructured surface of the working electrode. *Sens. Actuators B* **230**, 801–809 (2016).
17. T. Kawanishi, M. A. Romey, P. C. Zhu, M. Z. Holody, S. Shinkai, A study of boronic acid based fluorescent glucose sensors. *J. Fluoresc.* **14**, 499–512 (2004).
18. T. D. James, K. R. A. Samankumara Sandanayake, S. Shinkai, Chiral discrimination of monosaccharides using a fluorescent molecular sensor. *Nature* **374**, 345–347 (1995).
19. R. J. Russell, M. V. Pishko, C. C. Gefrides, M. J. McShane, G. L. Coté, A fluorescence-based glucose biosensor using concanavalin A and dextran encapsulated in a poly(ethylene glycol) hydrogel. *Anal. Chem.* **71**, 3126–3132 (1999).
20. J. Sawayama, S. Takeuchi, Long-term continuous glucose monitoring using a fluorescence-based biocompatible hydrogel glucose sensor. *Adv. Healthc. Mater.* **10**, 2001286 (2021).
21. H. Lee, T. K. Choi, Y. B. Lee, H. R. Cho, R. Ghaffari, L. Wang, H. J. Choi, T. D. Chung, N. Lu, T. Hyeon, S. H. Choi, D. H. Kim, A graphene-based electrochemical device with thermoresponsive microneedles for diabetes monitoring and therapy. *Nat. Nanotechnol.* **11**, 566–572 (2016).
22. Y. Yang, Y. Song, X. Bo, J. Min, O. S. Pak, L. Zhu, M. Wang, J. Tu, A. Kogan, H. Zhang, T. K. Hsiai, Z. Li, W. Gao, A laser-engraved wearable sensor for sensitive detection of uric acid and tyrosine in sweat. *Nat. Biotechnol.* **38**, 217–224 (2020).

23. W. Gao, S. Emaminejad, H. Y. Y. Nyein, S. Challa, K. Chen, A. Peck, H. M. Fahad, H. Ota, H. Shiraki, D. Kiriya, D. H. Lien, G. A. Brooks, R. W. Davis, A. Javey, Fully integrated wearable sensor arrays for multiplexed in situ perspiration analysis. *Nature* **529**, 509–514 (2016).
24. Y. Lin, M. Bariya, H. Y. Y. Nyein, L. Kivimäki, S. Uusitalo, E. Jansson, W. Ji, Z. Yuan, T. Happonen, C. Liedert, J. Hiltunen, Z. Fan, A. Javey, Porous enzymatic membrane for nanotextured glucose sweat sensors with high stability toward reliable noninvasive health monitoring. *Adv. Funct. Mater.* **29**, 1902521 (2019).
25. D. H. Keum, S. K. Kim, J. Koo, G. H. Lee, C. Jeon, J. W. Mok, B. H. Mun, K. J. Lee, E. Kamrani, C. K. Joo, S. Shin, J. Y. Sim, D. Myung, S. H. Yun, Z. Bao, S. K. Hahn, Wireless smart contact lens for diabetic diagnosis and *therapy*. *Advances* **6**, eaba3252 (2020).
26. W. D. Mathers, T. E. Daley, Tear flow and evaporation in patients with and without dry eye. *Ophthalmology* **103**, 664–669 (1996).
27. G.-H. Lee, H. Moon, H. Kim, G. H. Lee, W. Kwon, S. Yoo, D. Myung, S. H. Yun, Z. Bao, S. K. Hahn, Multifunctional materials for implantable and wearable photonic healthcare devices. *Nat. Rev. Mater.* **5**, 149–165 (2020).
28. E. Cengiz, W. V. Tamborlane, A tale of two compartments: Interstitial versus blood glucose monitoring. *Diabetes Technol. Ther.* **11**, S11–S16 (2009).
29. T. Kim, Y. Shin, K. Kang, K. Kim, G. Kim, Y. Byeon, H. Kim, Y. Gao, J. R. Lee, G. Son, T. Kim, Y. Jun, J. Kim, J. Lee, S. Um, Y. Kwon, B. G. Son, M. Cho, M. Sang, J. Shin, K. Kim, J. Suh, H. Choi, S. Hong, H. Cheng, H. G. Kang, D. Hwang, K. J. Yu, Ultrathin crystalline-silicon-based strain gauges with deep learning algorithms for silent speech interfaces. *Nat. Commun.* **13**, 5815 (2022).
30. H. Fang, K. J. Yu, C. Gloschat, Z. Yang, E. Song, C. H. Chiang, J. Zhao, S. M. Won, S. Xu, M. Trumpis, Y. Zhong, S. W. Han, Y. Xue, D. Xu, S. W. Choi, G. Cauwenberghs, M. Kay, Y. Huang, J. Viventi, I. R. Efimov, J. A. Rogers, Capacitively coupled arrays of multiplexed flexible silicon transistors for long-term cardiac electrophysiology. *Nat. Biomed. Eng.* **1**, 0038 (2017).
31. L. Tian, B. Zimmerman, A. Akhtar, K. J. Yu, M. Moore, J. Wu, R. J. Larsen, J. W. Lee, J. Li, Y. Liu, B. Metzger, S. Qu, X. Guo, K. E. Mathewson, J. A. Fan, J. Cornman, M. Fatina, Z. Xie, Y. Ma, J. Zhang, Y. Zhang, F. Dolcos, M. Fabiani, G. Gratton, T. Bretl, L. J. Hargrove, P. V. Braun, Y. Huang, J. A. Rogers, Large-area MRI-compatible epidermal electronic interfaces for prosthetic control and cognitive monitoring. *Nat. Biomed. Eng.* **3**, 194–205 (2019).
32. M. Sang, K. Kim, J. Shin, K. J. Yu, Ultra-thin flexible encapsulating materials for soft bio-integrated electronics. *Adv. Sci.* **9**, 2202980 (2022).
33. M. Mahmood, N. Kim, M. Mahmood, H. Kim, H. Kim, N. Rodeheaver, M. Sang, K. J. Yu, W. H. Yeo, VR-enabled portable brain-computer interfaces via wireless soft bioelectronics. *Biosens. Bioelectron.* **210**, 114333 (2022).
34. M. Sang, K. Kang, Y. Zhang, H. Zhang, K. Kim, M. Cho, J. Shin, J. H. Hong, T. Kim, S. K. Lee, W. H. Yeo, J. W. Lee, T. Lee, B. Xu, K. J. Yu, Ultrahigh sensitive Au-doped silicon nano-membrane based wearable sensor arrays for continuous skin temperature monitoring with high precision. *Adv. Mater.* **34**, 2105865 (2022).
35. J. Y. Lee, S. H. Park, Y. Kim, Y. U. Cho, J. Park, J. H. Hong, K. Kim, J. Shin, J. E. Ju, I. S. Min, M. Sang, H. Shin, U. J. Jeong, Y. Gao, B. Li, A. Zhumbayeva, K. Y. Kim, E. B. Hong, M. H. Nam, H. Jeon, Y. Jung, H. Cheng, I. J. Cho, K. J. Yu, Foldable three dimensional neural electrode arrays for simultaneous brain interfacing of cortical surface and intracortical multilayers. *npj Flex. Electron.* **6**, 86 (2022).
36. J. Shin, Y. Yan, W. Bai, Y. Xue, P. Gamble, L. Tian, I. Kandela, C. R. Haney, W. Spees, Y. Lee, M. Choi, J. Ko, H. Ryu, J. K. Chang, M. Pezhouh, S. K. Kang, S. M. Won, K. J. Yu, J. Zhao, Y. K. Lee, M. MacEwan, S. K. Song, Y. Huang, W. Z. Ray, J. A. Rogers, Bioresorbable pressure sensors protected with thermally grown silicon dioxide for the monitoring of chronic diseases and healing processes. *Nat. Biomed. Eng.* **3**, 37–46 (2019).
37. S. M. Yang, J. H. Shim, H. U. Cho, T. M. Jang, G. J. Ko, J. Shim, T. H. Kim, J. Zhu, S. Park, Y. S. Kim, S. Y. Joung, J. C. Choe, J. W. Shin, J. H. Lee, Y. M. Kang, H. Cheng, Y. Jung, C. H. Lee, D. P. Jang, S. W. Hwang, Hetero-integration of silicon nanomembranes with 2D materials for biore-sorbable, wireless neurochemical system. *Adv. Mater.* **34**, 2108203 (2022).
38. J. T. Reeder, Z. Xie, Q. Yang, M. H. Seo, Y. Yan, Y. Deng, K. R. Jinkins, S. R. Krishnan, C. Liu, S. McKay, E. Patnaude, A. Johnson, Z. Zhao, M. J. Kim, Y. Xu, I. Huang, R. Avila, C. Felicelli, E. Ray, X. Guo, W. Z. Ray, Y. Huang, M. R. MacEwan, J. A. Rogers, Soft, bioresorbable coolers for reversible conduction block of peripheral nerves. *Science* **377**, 109–115 (2022).
39. Y. S. Choi, R. T. Yin, A. Pfenniger, J. Koo, R. Avila, K. Benjamin Lee, S. W. Chen, G. Lee, G. Li, Y. Qiao, A. Murillo-Berlioz, A. Kiss, S. Han, S. M. Lee, C. Li, Z. Xie, Y. Y. Chen, A. Burrell, B. Geist, H. Jeong, J. Kim, H. J. Yoon, A. Banks, S. K. Kang, Z. J. Zhang, C. R. Haney, A. V. Sahakian, D. Johnson, T. Efimova, Y. Huang, G. D. Trachiotis, B. P. Knight, R. K. Arora, I. R. Efimov, J. A. Rogers, Fully implantable and bioresorbable cardiac pacemakers without leads or batteries. *Nat. Biotechnol.* **39**, 1228–1238 (2021).
40. Q. Yang, T. L. Liu, Y. Xue, H. Wang, Y. Xu, B. Emon, M. Wu, C. Rountree, T. Wei, I. Kandela, C. R. Haney, A. Brikha, I. Stepien, J. Hornick, R. A. Sponenburg, C. Cheng, L. Ladehoff, Y. Chen, Z. Hu, C. Wu, M. Han, J. M. Torkelson, Y. Kozorovitskiy, M. T. A. Saif, Y. Huang, J. K. Chang, J. A. Rogers, Ecoresorbable and bioresorbable microelectromechanical systems. *Nat. Electron.* **5**, 526–538 (2022).
41. K. J. Yu, D. Kuzum, S. W. Hwang, B. H. Kim, H. Juul, N. H. Kim, S. M. Won, K. Chiang, M. Trumpis, A. G. Richardson, H. Cheng, H. Fang, M. Thompson, H. Bink, D. Talos, K. J. Seo, H. N. Lee, S. K. Kang, J. H. Kim, J. Y. Lee, Y. Huang, F. E. Jensen, M. A. Dichter, T. H. Lucas, J. Viventi, B. Litt, J. A. Rogers, Bioresorbable silicon electronics for transient spatiotemporal mapping of electrical activity from the cerebral cortex. *Nat. Mater.* **15**, 782–791 (2016).
42. K. Tsioris, W. K. Raja, E. M. Pritchard, B. Panilaitis, D. L. Kaplan, F. G. Omenetto, Fabrication of silk microneedles for controlled-release drug delivery. *Adv. Funct. Mater.* **22**, 330–335 (2012).
43. H. Teymourian, F. Tehrani, K. Mahato, J. Wang, Lab under the skin: Microneedle based wearable devices. *Adv. Healthc. Mater.* **10**, 2002255 (2021).
44. S. Lau, J. Fei, H. Liu, W. Chen, R. Liu, Multilayered pyramidal dissolving microneedle patches with flexible pedestals for improving effective drug delivery. *J. Control. Release* **265**, 113–119 (2017).
45. W. Li, R. N. Terry, J. Tang, M. R. Feng, S. P. Schwendeman, M. R. Prausnitz, Rapidly separable microneedle patch for the sustained release of a contraceptive. *Nat. Biomed. Eng.* **3**, 220–229 (2019).
46. Z. Yin, D. Kuang, S. Wang, Z. Zheng, V. K. Yadavalli, S. Lu, Swellable silk fibroin microneedles for transdermal drug delivery. *Int. J. Biol. Macromol.* **106**, 48–56 (2018).
47. M. R. Prausnitz, R. Langer, Transdermal drug delivery. *Nat. Biotechnol.* **26**, 1261–1268 (2008).
48. G. Valdés-Ramírez, Y. C. Li, J. Kim, W. Jia, A. J. Bandodkar, R. Nuñez-Flores, P. R. Miller, S. Y. Wu, R. Narayan, J. R. Windmiller, R. Polsky, J. Wang, Microneedle-based self-powered glucose sensor. *Electrochem. Commun.* **47**, 58–62 (2014).
49. K. Kim, J.-B. Lee, High aspect ratio tapered hollow metallic microneedle arrays with mi-crofluidic interconnector. *Microsyst. Technol.* **13**, 231–235 (2006).
50. K. Lee, H. C. Lee, D.-S. Lee, H. Jung, Drawing lithography: Three-dimensional fabrication of an ultrahigh-aspect-ratio microneedle. *Adv. Mater.* **22**, 483–486 (2010).
51. H. Chang, M. Zheng, X. Yu, A. Than, R. Z. Seeni, R. Kang, J. Tian, D. P. Khanh, L. Liu, P. Chen, C. Xu, A swellable microneedle patch to rapidly extract skin interstitial fluid for timely metabolic analysis. *Adv. Mater.* **29**, 1702243 (2017).
52. P. M. Wang, M. Cornwell, M. R. Prausnitz, Minimally invasive extraction of dermal interstitial fluid for glucose monitoring using microneedles. *Diabetes Technol. Ther.* **7**, 131–141 (2005).
53. F. Tehrani, H. Teymourian, B. Wuerstle, J. Kavner, R. Patel, A. Furmidge, R. Aghavali, H. Hosseini-Toudeshki, C. Brown, F. Zhang, K. Mahato, Z. Li, A. Barfidokht, L. Yin, P. Warren, N. Huang, Z. Patel, P. P. Mercier, J. Wang, An integrated wearable microneedle array for the continuous monitoring of multiple biomarkers in interstitial fluid. *Nat. Biomed. Eng.* **6**, 1214–1224 (2022).
54. H. Shibata, Y. J. Heo, T. Okitsu, Y. Matsunaga, T. Kawanishi, S. Takeuchi, Injectable hydrogel microbeads for fluorescence-based in vivo continuous glucose monitoring. *Proc. Natl. Acad. Sci. U.S.A.* **107**, 17894–17898 (2010).
55. H. Zhang, H. Zhao, X. Zhao, C. Xu, D. Franklin, A. Vázquez-Guardado, W. Bai, J. Zhao, K. Li, G. Monti, W. Lu, A. Kobeissi, L. Tian, X. Ning, X. Yu, S. Mehta, D. Chanda, Y. Huang, S. Xu, B. E. Perez White, J. A. Rogers, Biocompatible light guide-assisted wearable devices for enhanced UV light delivery in deep skin. *Adv. Funct. Mater.* **31**, 2100576 (2021).
56. D. L. Heichel, N. C. H. Vy, S. P. Ward, D. H. Adamson, K. A. Burke, Controlled radical polymerization of hydrophilic and zwitterionic brush-like polymers from silk fibroin surfaces. *J. Mater. Chem. B* **8**, 10392–10406 (2020).
57. Q. Lu, B. Zhang, M. Li, B. Zuo, D. L. Kaplan, Y. Huang, H. Zhu, Degradation mechanism and control of silk fibroin. *Biomacromolecules* **12**, 1080–1086 (2011).
58. F. Mottaghitalab, M. Farokhi, M. A. Shokrgozar, F. Atyabi, H. Hosseinkhani, Silk fibroin nanoparticle as a novel drug delivery system. *J. Control. Release* **206**, 161–176 (2015).
59. T. Yucel, M. L. Lovett, D. L. Kaplan, Silk-based biomaterials for sustained drug delivery. *J. Control. Release* **190**, 381–397 (2014).
60. N. Ben Halima, Poly(vinyl alcohol): Review of its promising applications and insights into biodegradation. *RSC Advances* **6**, 39823–39832 (2016).
61. E. Chiellini, A. Corti, S. D'Antone, R. Solaro, Biodegradation of poly (vinyl alcohol) based materials. *Prog. Polym. Sci.* **28**, 963–1014 (2003).
62. Q. Wang, R. Zhao, S. Wang, H. Guo, J. Li, H. Zhou, X. Wang, X. Wu, Y. Wang, W. Chen, W. Zhang, A highly selective electrochemical sensor for nifedipine based on layer-by-layer assembly films from polyaniline and multiwalled carbon nanotube. *J. Appl. Polym. Sci.* **133**, (2016).
63. E. Lepore, M. Isaia, S. Mammola, N. Pugno, The effect of ageing on the mechanical properties of the silk of the bridge spider Larinioides cornutus (Clerck, 1757). *Sci. Rep.* **6**, 24699 (2016).
64. N. Jain, V. K. Singh, S. Chauhan, A review on mechanical and water absorption properties of polyvinyl alcohol based composites/films. *J. Mech. Behav. Mater.* **26**, 213–222 (2017).

65. S. Gupta, A. K. Pramanik, A. Kailath, T. Mishra, A. Guha, S. Nayar, A. Sinha, Composition dependent structural modulations in transparent poly(vinyl alcohol) hydrogels. *Colloids Surf. B Biointerfaces* **74**, 186–190 (2009).
66. S. Pan, M. Xia, H. Li, X. Jiang, P. He, Z. Sun, Y. Zhang, Transparent, high-strength, stretchable, sensitive and anti-freezing poly(vinyl alcohol) ionic hydrogel strain sensors for human motion monitoring. *J. Mater. Chem. C* **8**, 2827–2837 (2020).
67. T. E. Somesh, M. Q. A. Al-Gunaid, B. S. Madhukar, Siddaramaiah, Photosensitization of optical band gap modified polyvinyl alcohol films with hybrid AgAlO2 nanoparticles. *J. Mater. Sci. Mater. Electron.* **30**, 37–49 (2018).
68. H. Abral, J. Ariksa, M. Mahardika, D. Handayani, I. Aminah, N. Sandrawati, S. M. Sapuan, R. A. Ilyas, Highly transparent and antimicrobial PVA based bionanocomposites reinforced by ginger nanofiber. *Polymer Testing* **81**, 106186 (2020).
69. J. Pan, W. Ruan, M. Qin, Y. Long, T. Wan, K. Yu, Y. Zhai, C. Wu, Y. Xu, Intradermal delivery of STAT3 siRNA to treat melanoma via dissolving microneedles. *Sci. Rep.* **8**, 1117 (2018).
70. J. S. Kochhar, T. C. Quek, W. J. Soon, J. Choi, S. Zou, L. Kang, Effect of microneedle geometry and supporting substrate on microneedle array penetration into skin. *J. Pharm. Sci.* **102**, 4100–4108 (2013).
71. V. C. F. Mosqueira, P. Legrand, J. L. Morgat, M. Vert, E. Mysiakine, R. Gref, J. P. Devissaguet, G. Barratt, Biodistribution of long-circulating PEG-grafted nanocapsules in mice: Effects of PEG chain length and density. *Pharm. Res.* **18**, 1411–1419 (2001).
72. D. E. Discher, A. Eisenberg, Polymer vesicles. *Science* **297**, 967–973 (2002).
73. H. Lu, Z. Li, N. Hu, Direct voltammetry and electrocatalytic properties of catalase incorporated in polyacrylamide hydrogel films. *Biophys. Chem.* **104**, 623–632 (2003).
74. S. Fakhraei Lahiji, Y. Kim, G. Kang, S. Kim, S. Lee, H. Jung, Tissue interlocking dissolving microneedles for accurate and efficient transdermal delivery of biomolecules. *Sci. Rep.* **9**, 7886 (2019).
75. S. P. Davis, B. J. Landis, Z. H. Adams, M. G. Allen, M. R. Prausnitz, Insertion of microneedles into skin: measurement and prediction of insertion force and needle fracture force. *J. Biomech.* **37**, 1155–1163 (2004).
76. O. A. Shergold, N. A. Fleck, Experimental investigation into the deep penetration of soft solids by sharp and blunt punches, with application to the piercing of skin. *J. Biomech. Eng.* **127**, 838–848 (2005).
77. B. Aussedat, M. Dupire-Angel, R. Gifford, J. C. Klein, G. S. Wilson, G. Reach, Interstitial glucose concentration and glycemia: Implications for continuous subcutaneous glucose monitoring. *Am. J. Physiol. Endocrinol. Metabol.* **278**, E716–E728 (2000).
78. J. P. Bantle, W. Thomas, Glucose measurement in patients with diabetes mellitus with dermal interstitial fluid. *J. Lab. Clin. Med.* **130**, 436–441 (1997).
79. H. Lee, Y. J. Hong, S. Baik, T. Hyeon, D.-H. Kim, Enzyme-based glucose sensor: From invasive to wearable device. *Adv. Healthc. Mater.* **7**, 1701150 (2018).
80. H. Teymourian, A. Barfidokht, J. Wang, Electrochemical glucose sensors in diabetes management: an updated review (2010–2020). *Chem. Soc. Rev.* **49**, 7671–7709 (2020).

Acknowledgments

Funding: This study was funded by the National Research Foundation of Korea grant nos. NRF-2019R1A2C2086085, NRF-2021R1A4A1031437, and NRF-2018M3A7B4071109 (K.J.Y.); KIST Institutional Program Project no. 2E31603-22-140 (K.J.Y.); International Joint Research Grant by Yonsei Graduate School (K.J.Y.); Korea Medical Device Development Fund grant funded by the Korea government the Ministry of Science and ICT Project Number: KMDF_PR_20200901_0093, 9991006766 (T.L.); the National Research Foundation of Korea (NRF) funded by the Priority Research Centers Program through the National Research Foundation of Korea NRF-2019R1A6A1A11055660 (T.L.); and National Research Foundation of Korea grant no. NRF-2021R1A2C1009326 (Y.J.H.). **Author contributions:** M.S., M.C., S.L., I.S.M., Y.H., C.L., J.S., and K.Y. performed experiments and data analysis. W.-H.Y., T.L., and S.M.W. participated in the discussion of the methods. K.J.Y., Y.J.H., and Y.J. supervised and directed this work. M.S., M.C., S.L., I.S.M., Y.J., Y.J.H., and K.J.Y. wrote the manuscript. All authors discussed and commented on the manuscript. **Competing interests:** The authors declare that they have no competing interests. **Data and materials availability:** All data needed to evaluate the conclusions in the paper are present in the paper and/or the Supplementary Materials.

Submitted 15 February 2023
Accepted 24 April 2023
Published 31 May 2023
10.1126/sciadv.adh1765